Ocean Systems Engineering, *Vol. 8, No. 2 (2018) 223-246*
DOI: https://doi.org/10.12989/ose.2018.8.2.223

Water impact of three dimensional wedges using CFD

Vinod V. Nair and S.K. Bhattacharyya*

Department of Ocean Engineering, Indian Institute of Technology Madras, India

(Received March 14, 2018, Revised June 14, 2018, Accepted June 16, 2018)

Abstract. In this paper the results of CFD simulations, that were carried out to study the impact pressures acting on a symmetric wedge during water entry under the influence of gravity, are presented. The simulations were done using a solver implementing finite volume discretization and using the VOF scheme to keep track of the free surface during water entry. The parameters such as pressure on impact, displacement, velocity, acceleration and net hydrodynamic forces, etc., which govern the water entry process are monitored during the initial stage of water entry. In addition, the results of the complete water entry process of wedges covering the initial stage where the impact pressure reaches its maximum as well as the late stage that covers the rebound process of the buoyant wedge are presented. The study was conducted for a few touchdown velocities to understand its influence on the water entry phenomenon. The simulation results are compared with the experimental measurements available in the literature with good accuracy. The various computational parameters (e.g., mesh size, time step, solver, etc.) that are necessary for accurate prediction of impact pressures, as well as the entry-exit trajectory, are discussed.

Keywords: CFD; water entry; water impact; wedge

1. Introduction

The problem of water impact and subsequent water entry of rigid bodies has many marine engineering applications. For example, when a ship encounters rough sea condition, the well-known slamming phenomenon, which is a problem of water impact, induces very high loads on the ship structure and may mostly contribute to its local damage. Repeated slamming may also induce global effects such as whipping (Faltinsen 2005), which often leads to severe hull vibration and structural failure. The application of water impact as well as the subsequent water entry also extends to re-entry vehicles, crew exploration vehicles and ditching of aircraft, which upon landing on water must withstand impact loads, which may be high if the touchdown velocity is high. Hence, the water entry problem requires reliable prediction of the parameters influencing the initial as well as the subsequent stages of water entry.

The first literature reported on the problem of water impact was by von Karman (1929), who derived an analytical expression for the force of impact on a wedge-shaped body using momentum theorem. The rise in water surface during the water entry process, which was not considered by von Karman, was considered later by Wagner (1932) who showed that the rise in water surface causes an increase in impact force.

*Corresponding author, Professor, E-mail: skbh@iitm.ac.in

http://www.techno-press.org/?journal=ose&subpage=7 ISSN: 2093-6702 (Print), 2093-677X (Online)

Water entry of various shapes such as hemisphere, cone, wedge, cylinder, ship type bow flare section etc. have been discussed in the literature. In the present work, the water entry of three-dimensional wedges under free fall is considered. One of the earliest experiments on the wedge was by Bisplinghoff and Doherty (1952). They conducted drop tests on wedges made of wood, having deadrise angles 10°, 20°, 30°, 40° and 50°. Their work mainly focused on the photographic study of the piled-up water using a high-speed camera. They also reported the variation of acceleration with time, apparent mass ratio and maximum acceleration for various deadrise angles. Chuang (1966) experimentally investigated the free fall water entry of wedges (0.673 m length) with deadrise angles 1°, 3°, 6°, 10° and 15° and also a flat plate with focus on the air entrapped during the impact. It was reported that the wedge with deadrise angles 3° and more did not entrap much air. The variations of the maximum impact pressure with drop heights and deadrise angles were reported. Zhao *et al*. (1996) conducted drop test on a wedge (1 m length) with deadrise angle of 30° with the main aim to validate their numerical model and reported the time variations of velocity and hydrodynamic forces. Engle and Lewis (2003) conducted free fall experiments on wedges with deadrise angles 10° and 20° for various touchdown velocities varying from 1.25 m/s to 2.34 m/s and compared the maximum impact pressure variation with impact velocity using various hydrodynamic impact prediction methods. Carcaterra and Ciappi (2004) examined the hydrodynamic force and acceleration variations of free falling rigid wedge with a deadrise angle of 30° having impact velocities 1.5 m/s, 3 m/s and 5 m/s. Wu *et al.* (2004) performed drop tests on wedges (0.6 m length) with deadrise angles 20° and 45° and mainly reported the time variation of acceleration for various touchdown velocities and wedge mass. They compared their experimental results with their numerical formulation and found better agreement with the 45° wedge as compared to the 20° wedge. Judge *et al*. (2004) experimentally studied the vertical as well as oblique water entry of symmetric and asymmetric wedges (0.46 m length) with a deadrise angle of 37°. Their work mainly focused on the water entry of wedges with small as well as large asymmetry and provided high-speed camera images of water entry with these asymmetries at a few horizontal velocities. Yettou *et al.* (2006) performed extensive experiments on wedges (1.2 m length) with deadrise angles 15°, 20°, 25°, 30° and 45°. They studied the effects of mass, deadrise angle, and the impact velocity and reported time variations of displacement, velocity and pressure. They also presented the variation of pressure as a function of dimensionless entry depth for various mass, drop height and deadrise angles and concluded that the effect of deadrise angle on the pressure is more predominant than that of the mass and impact velocity. Tvietnes *et al*. (2008) conducted constant velocity water entry and water exit experiments on wedges (0.3 m length) with deadrise angles 5°, 10°, 15°, 30° and 45° and measured the water entry and exit forces, added mass coefficient and hydrodynamic entry force coefficient as a function of non-dimensional penetration depth. The constant impact velocities used for the wedges was from 0.24 m/s to 1.19 m/s for the water entry problems and from 0.48 to 0.94 m/s for the water exit problems. Lewis *et al*. (2010) performed drop tests on two wedges (0.735 m length), both with deadrise angle 25° and one with a mass 23.4 kg and the other with a mass of 33.4 kg at two drop heights of 0.5 m and 0.75 m. They measured the variations of displacement, velocity, acceleration and pressure with time for the two wedges using a high-speed camera, pressure sensors and accelerometer based measurements. High- quality images of water entry of the wedges for two drop heights were also presented.

The water entry of rigid bodies has been studied analytically based on Wagner's theory and asymptotic solutions have been found for bodies of various shapes. Analytical study of water entry problem started with von Karman (1929) and Wagner (1932), and continued much later by

Greenhow (1987), Miloh (1991) and Zhao and Faltinsen (1993). An extensive review of the slamming studies was reported by Korobkin and Pukhnachov (1988). Even though a great deal of progress has been made in this area, difficulties in prediction arise when there is a high deformation of the free surface or when the free surface breaks. These difficulties can be overcome by using the Computational Fluid Dynamics (CFD) techniques, solving the Navier-Stokes equations by incorporating Volume of Fluid (VOF) method or other free surface tracking methods to track the free surface.

Muzaferija *et al.* (1998) studied the water entry of 2D and 3D wedges using CFD and compared the computed vertical hydrodynamic force with the experimental results of Zhao et al. (1996). Kleefsman *et al*. (2005) studied two-dimensional (2D) water impact problems of wedges using the VOF method with finite volume discretization. The velocity and vertical force variations of the 30° wedge were compared with the experimental results of Zhao *et al*. (1996). Chen *et al.* (2014) also studied the water entry of 2D wedge with experimental verification with the results of Yettou *et al.* (2006). Aquelet *et al*. (2006) simulated the water entry of a 2D wedge using the finite element method (FEM) in conjunction with Arbitrary Lagrangian Eulerian (ALE) method for fluid-structure coupling. The pressure distribution and force variation were reported and compared with the theoretical values of Zhao and Faltinsen (1993). Stenius *et al*. (2006) simulated water entry of a 2D wedge using FEM and plotted the pressure variations, but did not compare the results with experiments. Fairlie-Clarke and Tveitnes (2008) used finite volume discretization with VOF method to track the free surface for simulating the constant velocity water entry of 2D wedges of various deadrise angles and compared the maximum pressure coefficients as a function of the deadrise angle with the experimental results of Chuang (1967). Zhang *et al.* (2010) used the level set method to simulate 2D water entry of wedges. The variations of the velocity, vertical slamming forces, and pressure distribution were presented and compared with the experimental results of Zhao *et al.* (1996). Luo *et al.* (2011) used explicit FEM to simulate constant velocity water entry of a 2D wedge and compared the results of slamming loads and pressure distribution on the body at different time instants with the experimental results of Zhao *et al*. (1996). Yang and Qiu (2012a) used the CIP method to simulate the water entry of 2D wedge and compared the variation of vertical force with the experimental results of Zhao *et al.* (1996) and the maximum pressure coefficient as a function of the deadrise angle with the experimental results of Chuang (1967). This work on the 2D wedge was extended to 3D wedge by the same authors (Yang and Qiu 2012b).

Meshless methods such as smoothed particle hydrodynamics (SPH) has been used to investigate the water entry of wedges in Oger *et al*. (2006) and Gong *et al*. (2009). An extensive review of water entry with application to hull slamming is by Abrate (2013), which also deals with CFD techniques in studying the water entry problem.

From the survey of the literature presented above, it is found that most works on numerical simulation of water entry of wedges adopted 2D models, except the works of Muzaferija *et al.* (1998) and Yang and Qiu (2012b), who adopted 3D models. Only three papers (Aquelet *et al.* 2006, Luo *et al.* 2011 and Chen *et al.* 2014), all using 2D models, report time histories of impact pressures on wedges. However, two papers that adopted 3D models did not present the time history of impact pressure, the maximum value of which is an important parameter in the design.

In this present work, the water entry of 3D wedge is analyzed using the CFD approach based on Reynolds-averaged Navier-Stokes equations in conjunction with the VOF scheme to keep track of the free surface. Attempt has been made to correlate the predicted impact pressure as a function of time on the surface of the body, which is a measure of the degree of slamming, with the results

with experimental data available in the literature (Yettou *et al.* 2006). Especially, the prediction of the peak impact pressure, which is the most important parameter in practical systems, and its experimental validation is given special attention in the present work. Another objective of the present work is to predict the parameters influencing the water entry process during both 'early' stage where impact and inertia forces dominate as well as the 'late' stage where the buoyancy and viscous forces dominate, with experimental verification.

2. CFD theory

The commercial CFD solver FLOW3D (User manual, 2013) has been chosen for the present study, which uses a fixed mesh method for general moving objects and hence eliminating the complexities of moving mesh and deforming mesh. The fixed mesh method also helps in reducing the computational time. The conventional CFD solver mainly depends on deforming or the moving mesh to accommodate moving objects. The moving and deforming mesh places a limitation on the distance between the object and the water in the context of water entry problems. Also, the simulation fails if the mesh deformation is too large. Re-meshing and automatic mesh regeneration after certain time steps helps to address a few complexities in this regard but it becomes very much computationally expensive.

The GMO model uses the FAVOR (Fractional Areas/Volume Obstacle Representation) based technique to describe the geometric objects in a given simulation domain by making use of area fraction (AF) and volume fraction (VF) in Cartesian meshes (Sicilian 1990). The volume fraction is defined as the ratio of the open volume to the total volume in a mesh cell. The three area fractions (AFR, AFB, and AFT) are defined respectively at the three cell faces in the increasing cell index directions as the ratio of the open area to that of the total area. This technique introduces the AF and VF into the conservation equations in order to include the effect of various geometries. At every time step, the area and volume fractions are calculated to describe the updated location of the object and its orientation in the fixed rectangular mesh (Wei 2005a). In order to account for the fluid displacement due to the moving objects an additional source term is included in both continuity equation and VOF transport equation. To include the effect of object boundaries, the tangential velocity of the object is introduced in the shear stress terms in the momentum equation.

The equations of motion of the rigid body are

$$\vec{F} = m\frac{d\vec{V}}{dt} \text{ and } \vec{M} = [I]\frac{d\vec{\Omega}}{dt} + \vec{\Omega}\times\left([I]\vec{\Omega}\right) \tag{1}$$

where $\vec{F}$ and $\vec{M}$ are the force and moment (about the mass center G of the body) vectors respectively, m is the mass of the body, $[I]$ is the moment of inertia tensor of the body and $\vec{V}$ and $\vec{\Omega}$ are the translational and rotational velocity vectors of the body respectively. The velocity of a point on the surface of the body, $\vec{V}_B$, can be obtained from

$$\vec{V}_B = \vec{V} + \vec{\Omega}\times\vec{r} \tag{2}$$

where $\vec{r}$ is the vector from G to the point.

The continuity equation of fluid motion is

$$\frac{\partial \rho}{\partial t} + \nabla.\left(\rho \vec{u}\right) = S \tag{3}$$

where $\vec{u}$ is the fluid velocity vector, ρ is the fluid density and S is the mass source. In FAVOR method, the continuity equation can be interpreted as

$$\frac{\partial\left(\rho V_f\right)}{\partial t} + \nabla.\left(\rho \vec{u} A_f\right) = S_m \tag{4}$$

Where V_f and A_f are the volume and area fractions respectively and S_m is the physical mass source term of the fluid. In case of moving objects (GMO), V_f and A_f vary with time and this effect on the fluid flow must be considered. Eq. (4) can be written as

$$\frac{V_f}{\rho}\frac{\partial \rho}{\partial t} + \frac{1}{\rho}\nabla.\left(\rho \vec{u} A_f\right) = -\frac{\partial V_f}{\partial t} + \frac{S_m}{\rho} \tag{5}$$

Comparing the above with Eq. (3) shows that the term $-\partial V_f / \partial t$ is equivalent to an additional volume source. In finite volume method of discretization, this source term exists only in mesh cells around the boundary of the moving object. In the water entry problem, there is no physical mass source and therefore $S_m = 0$. Also, the fluid can be considered incompressible and therefore $\partial \rho / \partial t = 0$. As a result, Eq. (5) reduces to

$$\nabla.\left(\vec{u} A_f\right) = -\frac{\partial V_f}{\partial t} \tag{6}$$

Wei (2005) gave a new approximation for the volume source term due to the presence of the moving object as

$$\frac{\partial V_f}{\partial t} = \frac{S_B}{V_c}\vec{V}_B.\vec{n} \tag{7}$$

where, S_B is the surface area of the finite volume cell of the mesh on the boundary of the GMO in contact with the fluid, V_c is the volume of the finite volume cell of the mesh, $\vec{V}_B$ (see Eq. (2)) is at the cell and $\vec{n}$ is the unit normal vector of the surface of the GMO at the cell.
Substitution of Eq. (7) in Eq. (6) gives

$$\nabla.\left(\vec{u} A_f\right) = -\frac{S_B}{V_c}\vec{V}_B.\vec{n} \tag{8}$$

which is the continuity equation that is solved in the present approach to the water entry problem.

The momentum equation is

$$\frac{\partial \vec{u}}{\partial t} + \frac{1}{V_f}\left(\vec{u} A_f\right).\nabla \vec{u} = \vec{X} - \frac{1}{\rho}\nabla p - \frac{1}{\rho}\nabla.\left(\tau A_f\right) \tag{9}$$

where p is pressure, τ is the viscous stress tensor and $\vec{X}$ is the body force vector.

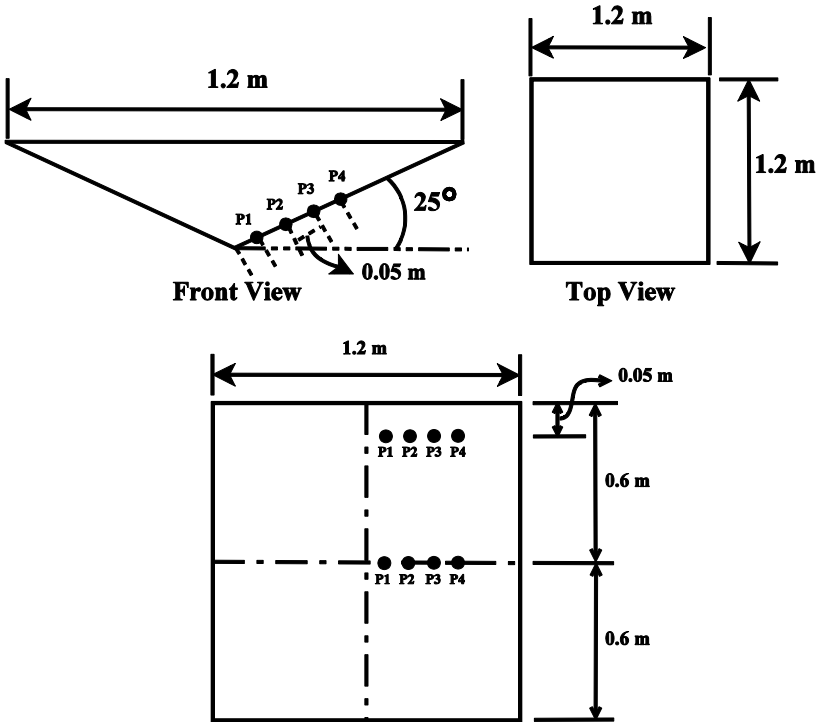

Fig. 1 Schematic diagram of the wedge and the location of the monitoring points

The transport equation for VOF function F (fluid fraction) is

$$\frac{\partial F}{\partial t}+\frac{1}{V}\nabla.\left(F\vec{u}A_f\right)=-\frac{F}{V_f}\frac{\partial V_f}{\partial t} \tag{10}$$

Since in the water entry problem, the simulation adopts an 'incompressible flow with sharp interface' option where the object is dropped from 'void' under gravity to touchdown on the water surface , F =1 represents region occupied by the water and F = 0 represents 'void' region, i.e. no fluid is present in that region.

During simulation, the equations of motion of the rigid body given in Eq. (1) are solved at each time step. The position, orientation and the area of volume fractions of the body (i.e., GMO) are calculated. The continuity equation, momentum equation and the VOF transport Eqs. (8)-(10) are solved numerically using an implicit solver.

3. Geometry, domain description and solver parameters

3.1 Geometry description

Four wedges of deadrise angle 15°, 20°, 25° and 30° are considered in the present study. The

schematic diagrams of the 25° wedge, showing the locations of the pressure monitoring points on their surfaces are shown in Fig. 1. The wedge is modeled to mimic the drop test experiments in a tank by Yettou *et al.* (2006). The inertia properties of the wedges are given in Table 1. The pressure monitoring probes are kept at two separate locations, one at the midsection of the wedge and the other at 50 mm from the edge of the wedge as shown in Fig. 1.

The initial velocity or the drop height and the moment of inertia tensor $[I]$ are given as an input to the solver. Simulations were performed to investigate the effect of deadrise angles and touchdown velocity (V_0). The initial stage of water entry and the subsequent stages were studied and the simulation results are validated with experimental results from the literature.

3.2 Domain description

Two domains were used to investigate the water entry problem of wedges, one designated Domain 1 for calculating the full motion (i.e., early as well as late stages) of the wedge and the other designated Domain 2 for calculating the early stage of water entry.

Domain 1 or the full domain is shown in Fig. 2(a) and it measures 6 m × 2 m × 2.5 m in the *x*, *y* and *z*-directions respectively, which is the size of the rectangular tank used in the experiments by Yettou *et al*. (2006). The water depth used in the experiments as well as the simulation is 1 m. The wedge is released from a certain height above the free surface in order to achieve the desired touchdown velocity V_0. The Domain 2 or the half domain, shown in Fig. 2(b), uses the symmetry of the wedge and it measures 2.4 m × 2 m × 1.5 m in the *x*, *y* and *z*- directions respectively.

The Domain 1 is discretized with hexahedral elements, with the edge length of elements being 20 mm uniformly and consists of about 4.14 million cells. The Domain 2 uses a finer mesh size, which is very essential to capture the impact pressure, which will be bought out later. An interaction region was identified, consisting of the region GHIJ measuring 2.4 m × 2 m × 0.4 m and the region ALKC measuring 0.6 m × 2 m × 1.5 m (see Fig. 2(b)). The interaction region has been uniformly discretized using hexahedral elements with edge length 5 mm. Coarser mesh sizes has been used in the other regions by using a suitable increment in mesh size (growth ratio has been chosen as 1.2) so that at the boundaries the maximum edge length used was about 55 mm. The mesh is shown in Fig. 2(c). The total number of cells in Domain 2 is approximately 4.79 million.

Table 1 The mass and inertial properties of the wedges

	Mass (kg)	CG (m) (from apex)	I_{xx} (kg·m^2)	I_{yy} (kg·m^2)	I_{zz} (kg·m^2)
15° wedge	89	0.1072	10.808	5.468	16.02
20° wedge	89	0.1456	10.916	5.576	16.02
25° wedge	94	0.1865	11.688	6.048	16.92
30° wedge	99	0.2309	12.54	6.6	17.82

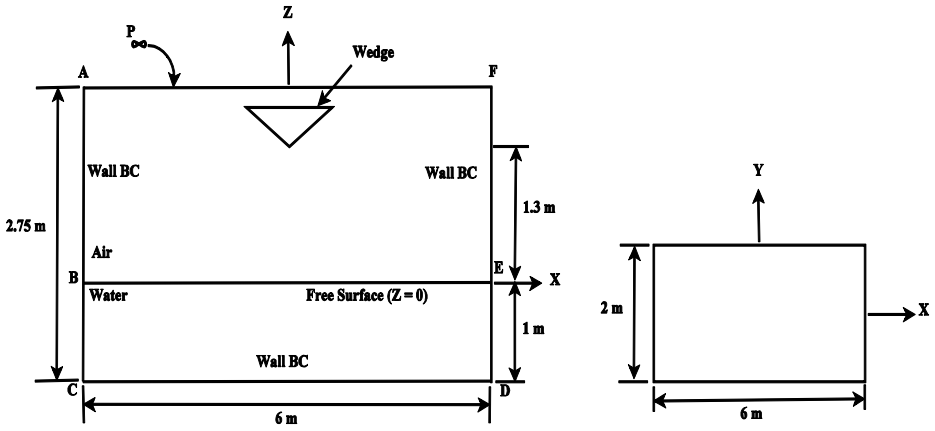

(a) Schematic diagram of Domain 1

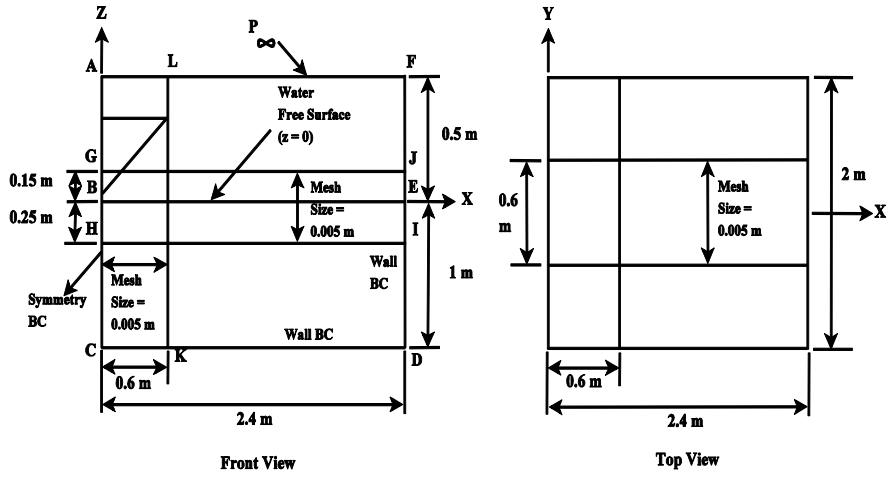

(b) Schematic diagram of Domain 2

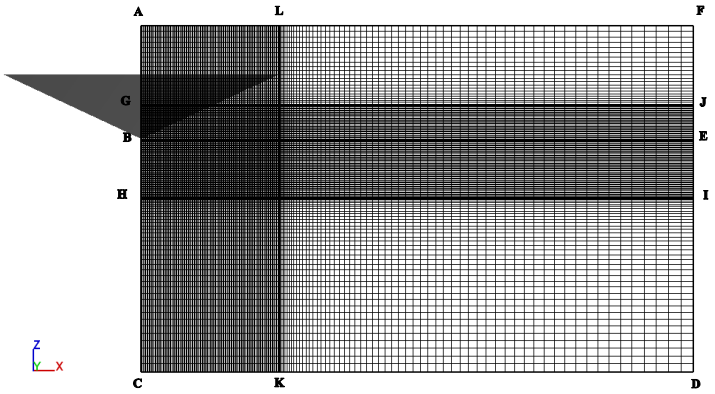

(c) Mesh of Domain 2

Fig. 2 Schematic diagram of the domains used for the water entry analysis of wedge

3.3 Boundary conditions

The boundary conditions (BCs) were assigned in such a way that they resemble the boundary conditions in the experiments. For all the four domains, the top boundary (AF in Fig. 2) was assigned 'Specified Pressure' BC with a value of 101325 N/m^2 (= P_∞) in order to account for the atmospheric pressure. For the full domain, i.e. Domain 1, all the boundaries AC, CD and DF were assigned 'Wall' BC in order to resemble the tank walls. For the half domain, i.e., Domain 2, the boundary conditions are specified as 'Symmetry' in the symmetry plane (AC in Fig. 2(b) in XZ plane), 'Wall' boundary condition is specified on all other boundaries.

The fluid was assumed incompressible. For the Domain 1, the flow was assumed turbulent since it is aimed to capture the full penetration depth and subsequent vertical oscillations where viscous forces are expected to be significant. For the Domain 2, the flow can be assumed either inviscid or laminar since this model is used to capture early time behaviour where viscous forces are expected to be insignificant compared to the inertial and impact forces. For the Domain 1 all degrees of freedom were allowed. For the Domain 2, only the vertical (or Z) translational degree of freedom was allowed in order to mimic the experimental condition of controlled water entry.

3.4 Solver parameters

The touchdown velocity (V_0) is defined as the velocity with which the body first touches the water surface. For early stage water entry problems, the bodies were kept at a distance of 0.01 m above the free surface of water and an initial velocity was specified such that the body achieves the desired touchdown velocity under the influence of gravity (g = 9.81 m/s^2). For a body to achieve a touchdown velocity of 5.05 m/s, an initial velocity of 5.03 m/s was specified.

A nominal time step of 2×10^{-5} s was used in all early stage water entry simulations. The pressure is solved using the implicit solver using the iterative Generalized Minimum Residual (GMRES) method. 'One fluid-sharp interface' option was specified for the VOF advection scheme (FLOW3D user manual, 2013).

4. Convergence study

The mesh convergence study was carried out using three mesh sizes for the Domain 2. The hexahedral mesh sizes in the interaction region were of edge lengths of 9 mm, 5 mm and 3 mm. The number of cells for these four mesh sizes was about 1.2 million for 9 mm, 4.8 million for 5 mm and 12.3 million for a 3 mm edge length. For a touchdown velocity of 5.05 m/s, the variation of pressure at the location P1 with time is plotted in Fig. 3(a) for mesh sizes 9 mm, 5 mm and 3 mm. The results, especially the peak pressure, are widely different for 9 mm and the 5 mm mesh size, but the peak pressures are almost identical in case of 5 mm and 3 mm mesh size. It will be shown later that the computed pressure using the mesh sizes 5 mm and 3 mm matches best with the experimental result. The 5 mm mesh size is chosen for the present study since this mesh size produces accurate results with less computational effort. The 3 mm mesh size took a computational time of 28 h 52 min for a total simulation time of 0.042 s while the 5 mm mesh size took 10 h 40 min for the same simulation time.

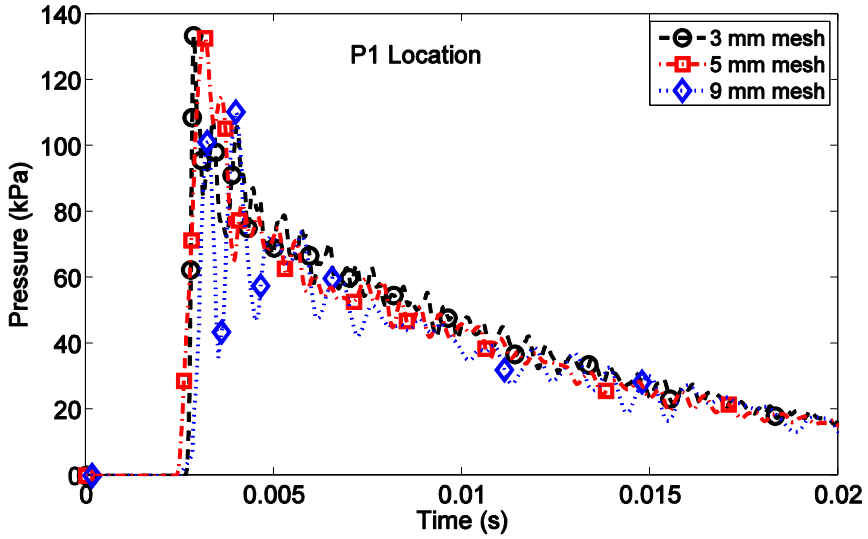

(a) Pressure variation with time at P1 location for various mesh sizes

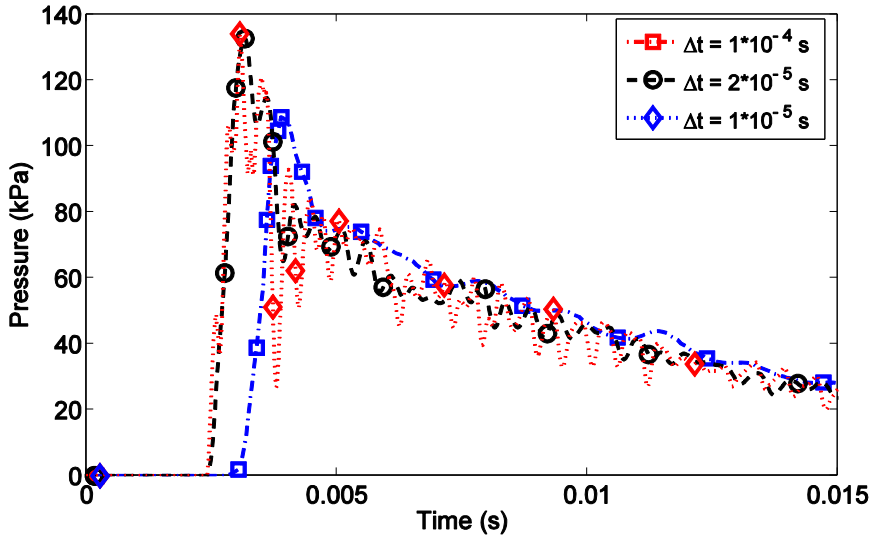

(b) Pressure variation with time at P1 location for various time steps

Fig. 3 Mesh size and time step convergence study for 25° wedge (V_0 = 5.05 m/s)

The accuracy of the solution also depends on the appropriate choice of the time step. The present solver uses an adaptive time stepping scheme wherein a nominal time step is an input by the user. The solver adjusts this time step, if needed, in accordance with the physics of the problem to keep the simulation in the numerically stable range so that convergence is assured. The pressure variations at P1 for three nominal time steps, 1×10^{-5} s, 2×10^{-5} s and 1×10^{-4} s are shown in Fig.

3(b), from which it is seen that the nominal time step is the upper bound of the adaptive time step. The peak pressure predicted are p = 132.7 kPa and 134.1 kPa for the nominal time steps of 2×10^{-5} s and 1×10^{-5} s respectively, and p = 108.8 kPa for the nominal time step of 1×10^{-4} s, the experimental value being p = 132.6 kPa. Clearly, the nominal time steps of 2×10^{-5} s and 1×10^{-5} s predict the peak pressure accurately and, therefore, a nominal time step of 2×10^{-5} s has been chosen in all calculations for initial stage water entry of wedges.

Finally, it should be pointed out that all pressure time histories in all calculations presented in this paper have been obtained by filtering the CFD results using an FIR filter wherein all frequencies above 10 Hz are removed and data is smoothed by a moving average technique, namely, a robust local regression using weighted linear least squares technique, subsequently.

5. Results

5.1 Early motion: validation with experiments

The CFD simulations were carried out for the early stage of water entry (up to 40 ms) of a 25° wedge with a touchdown velocity V_0 = 5.05 m/s. The mesh, nominal time step, simulation time and computation time are given in Table 2. The Courant number ($C = u\Delta t / \Delta x$) calculated on the basis of the touchdown velocity ($u = V_0$) is 0.02.

The velocity and pressure variations at the locations P1, P2, P3 and P4 (see Fig. 1) with time are compared with the experiment results reported by Yettou et al. (2006) in Fig. 4. The velocity variation shows reasonably accurate match and so do the pressure variations at all four locations. The peak pressures and their time instances of occurrence at P1, P3 and P4 are well predicted by the present CFD approach but it predicted about 16% lower peak pressure at P2, probably because of digitisation error from the experimental graph as well as measurement inaccuracies related to interaction of the wedge with the deforming free surface.

Table 2 Key parameters of the CFD set up for wedge

	Wedge
Edge length of cells inthe interaction region	5 mm
Nominal time step	2×10^{-5} s
Z-extent of the interaction region	0.4 m
Simulation time	0.045 s
Computation time	11 hr
Courant number, C	0.02
(V_0)	(5.05 m/s)
Circumferential mesh density (no. of elements per degree)	1.5

Simulations were carried out three touchdown velocities, V_0 = 6.26 m/s, 5.05 m/s and 4.43 m/s, which corresponds to drop heights h = 2 m, 1.3 m and 1 m respectively. The time variation of penetration depth, velocity, pressure, and total hydrodynamic force are presented in Fig. 5. The effect of touchdown velocity on the water entry process can be clearly understood from the pressure and force time histories plotted in Figs. 5(c) and 5(d) respectively, and it depicts that as the touchdown velocity increases, the maximum impact pressure and the total hydrodynamic force acting on the body increases.

Simulations for wedges with deadrise angles β = 15°, 20°, 25° and 30° (see Table 1) were carried out to understand its effect on the early stage of water entry. All wedges have the same top square section of size 1.2 m × 1.2 m (see Fig. 1). The computed results of the pressure and vertical hydrodynamic force time are shown in Fig. 6 showing a significant decrease of the peak pressure with an increase of the deadrise angle.

The three dimensional effect of the wedge is brought out using the present CFD study in Fig. 7 where the pressure time histories at midsection (i.e., at middle of the length of the wedge, 0.6 m from either end, see Fig. 1) and at a section 50 mm from one of the ends (see Fig. 1) are compared at all four monitoring points. Since water can flow around the ends of the wedge, it is expected that pressures, as well as their peak values near the ends, will be lower than the corresponding values away from the ends. This is clearly demonstrated in Fig. 7. The pressure contours on the inclined wall of the wedge are shown in Fig. 8 for a few instances of time. They clearly show that the two end regions have lower pressures than the regions away from the ends towards the midsection. A two-dimensional calculation, which had been popular in the literature, will not be able to capture these three-dimensional details of the pressure field on the body.

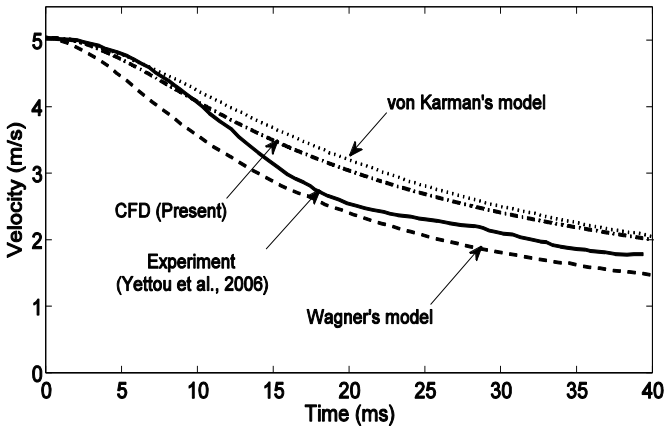

(a) Velocity variation with time

Continued-

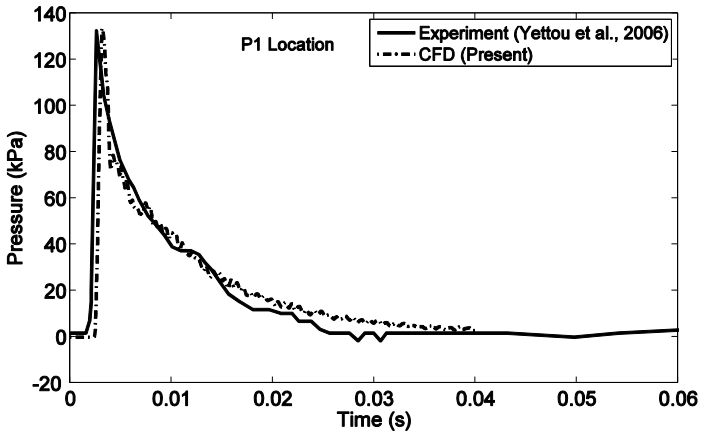

(b) Pressure variation with time at P1 location

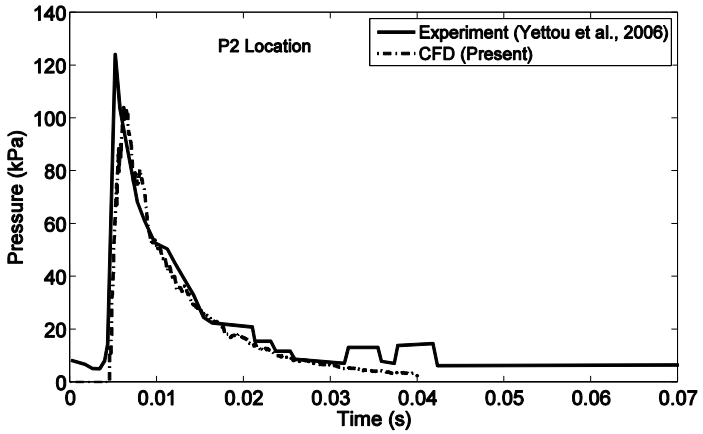

(c) Pressure variation with time at P2 location

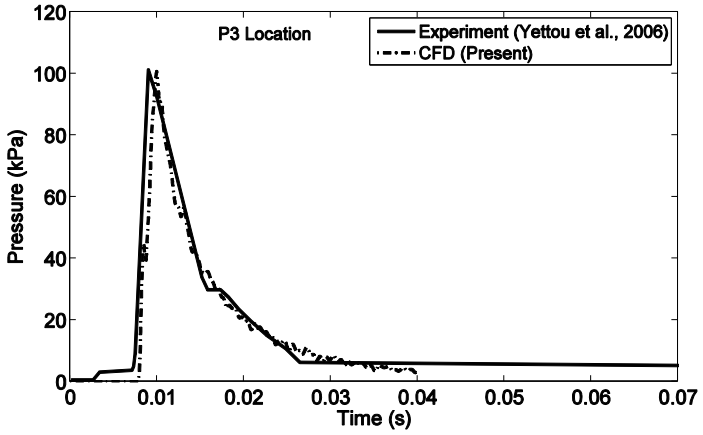

(d) Pressure variation with time at P3 location

Continued-

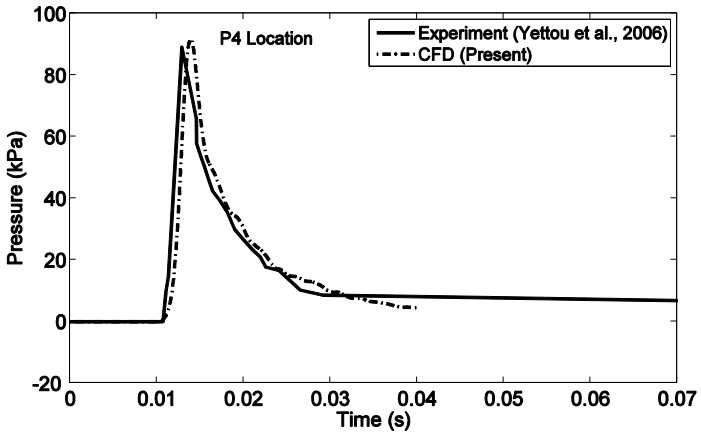

(e) Pressure variation with time at P4 location

Fig. 4 Comparison of CFD results with experiments for water entry of 25° wedge (V_0 = 5.05 m/s)

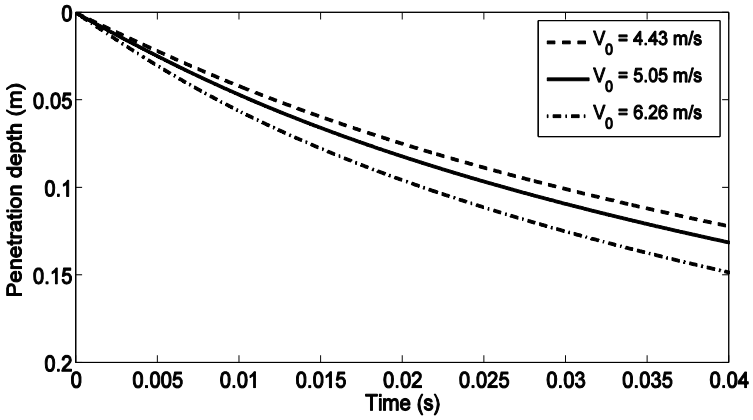

(a) Penetration depth variation with time

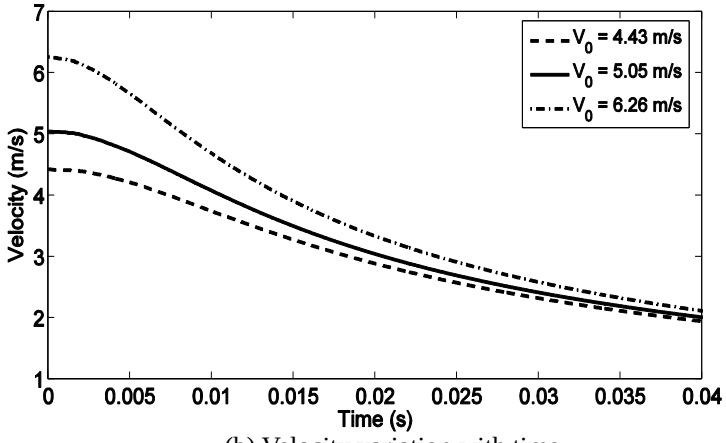

(b) Velocity variation with time

Continued-

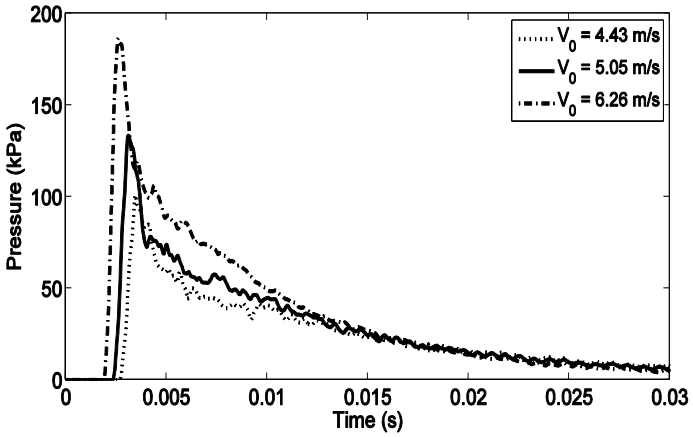

(c) Pressure variation with time at P1 location

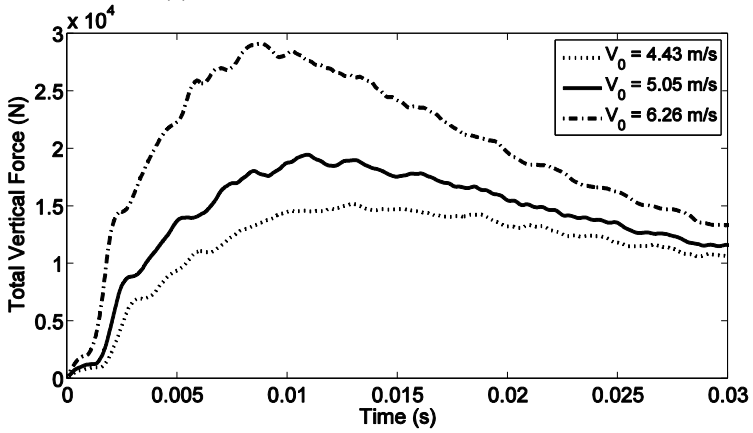

(d) Vertical force variation with time

Fig. 5 CFD simulation results for water entry of 25° wedge for three touchdown velocities

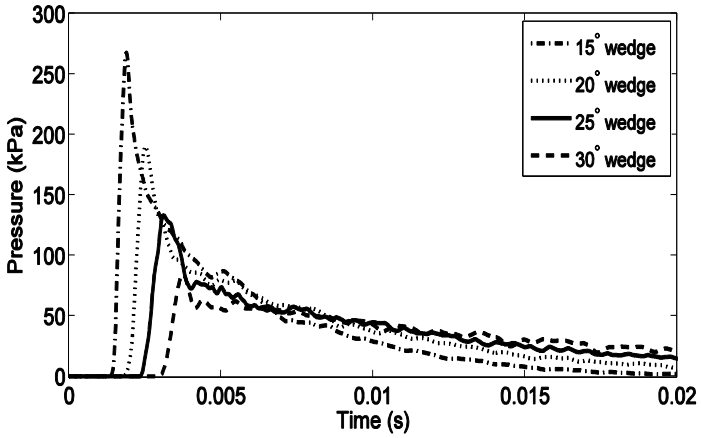

(a) Pressure variation with time at P1 location

Continued-

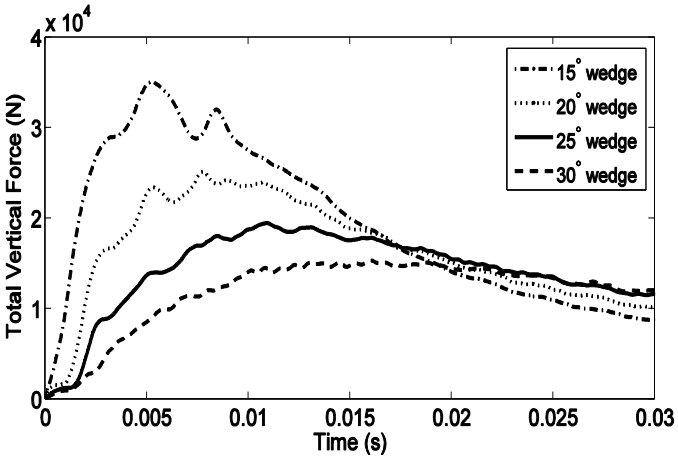

(b) Vertical force variation with time

Fig. 6 CFD simulation results for water entry of wedge with various deadrise angles

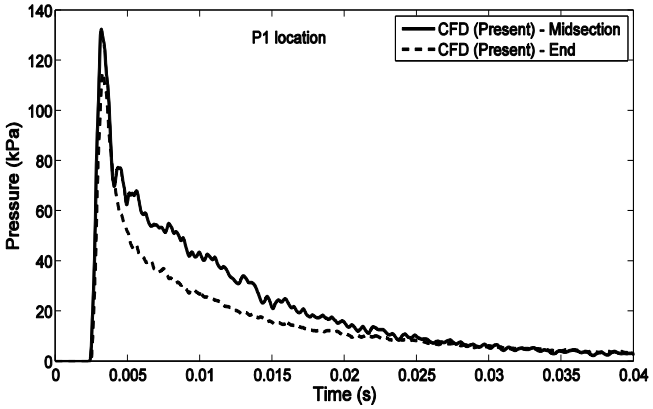

(a) Pressure variation with time at P1 location

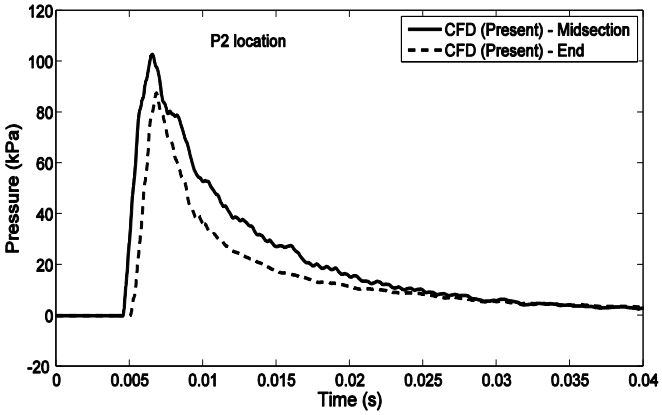

(b) Pressure variation with time at P2 location

Continued-

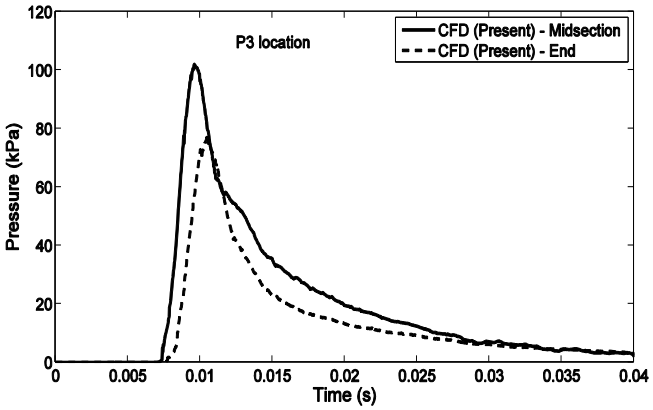

(c) Pressure variation with time at P3 location

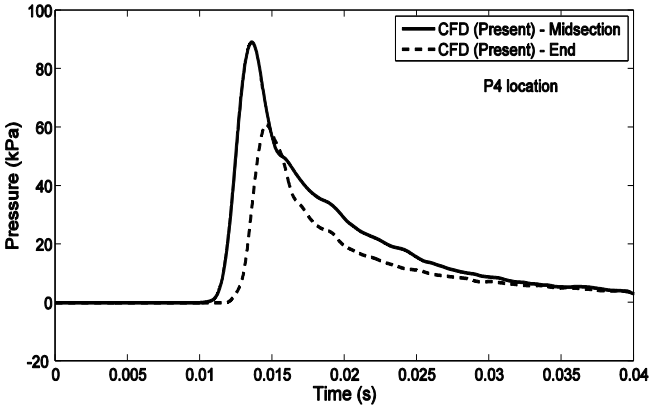

(d) Pressure variation with time at P4 location

Fig. 7 CFD simulation results of pressure at the midsection and near the end for water entry of 25° wedge (V_0 = 5.05 m/s)

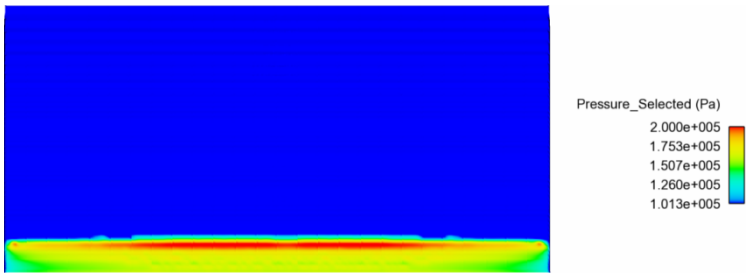

(a) t = 0.004 s

Continued-

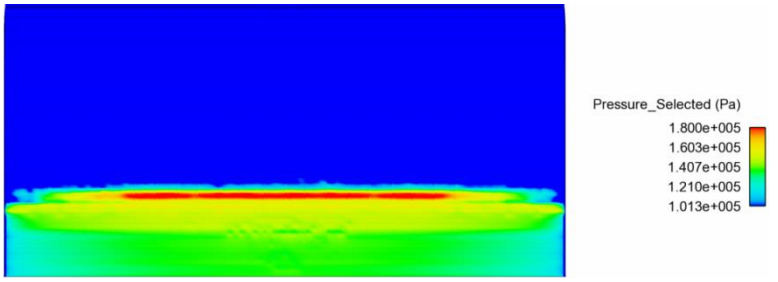

(b) t = 0.0114 s

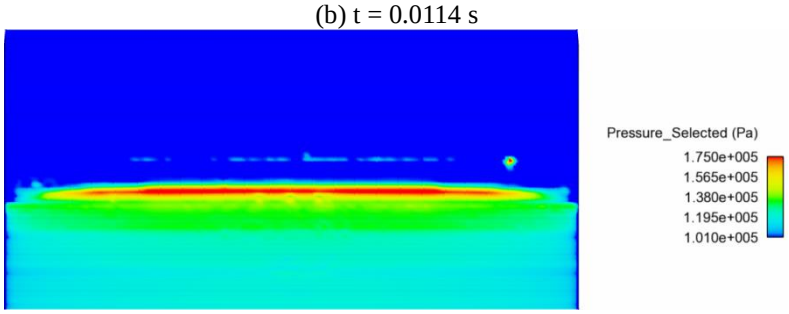

(c) t = 0.018 s

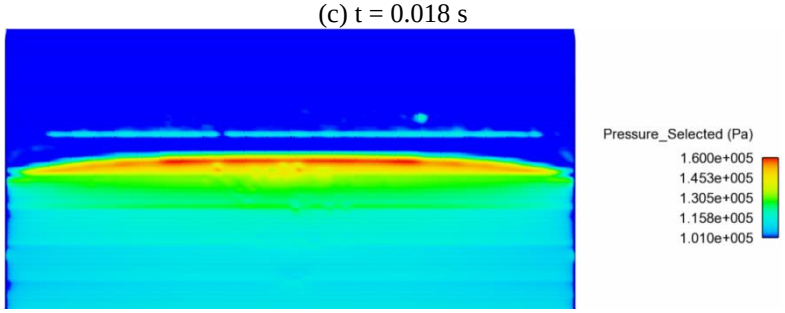

(d) t = 0.024 s

Fig. 8 CFD images showing the pressure contours on the inclined surface of the wedge during water entry of 25° wedge (V_0 = 5.05 m/s)

t = 0 s

t = 0.008 s

t = 0.019 s

t = 0.024 s

t = 0.025 s

t = 0.026 s

Continued-

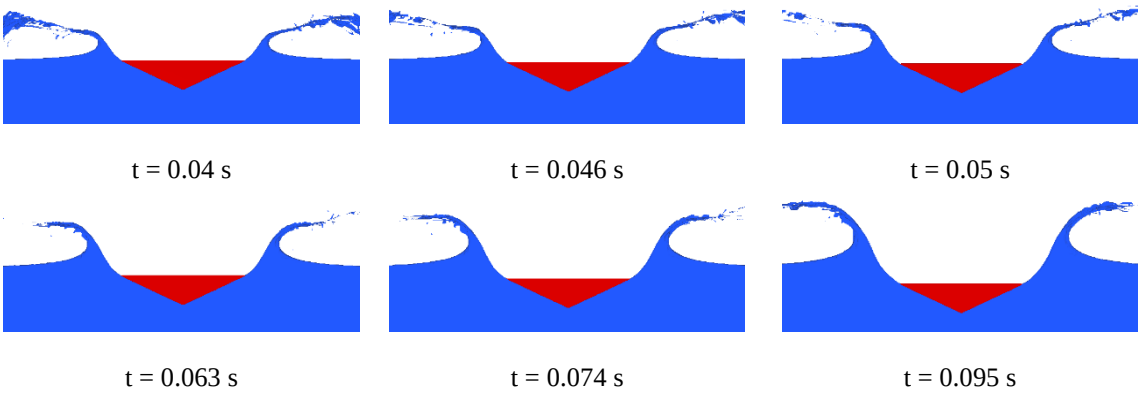

Fig. 9 Breaking of the free surface during water entry of 25° wedge (V_0 = 5.05 m/s)

5.2 Full motion: validation with experiments

The 25° wedge was kept at a distance of 1.3 m (= *h*) above the free surface and was allowed a free fall in a rectangular tank similar to the one used in the experiments and the simulation was carried out for several cycles of entry and rebound phases using the mesh of the Domain 1. The rebound phase, which happens because the wedge buoyant, is akin to the water exit problem. All degrees of freedom of the wedge were allowed. A computational time of nearly 5 hours was required for a simulation time of 3 s.

The comparisons of CFD results with experimental results of displacement and velocity variation with time are shown in Fig. 10, showing an accurate match. There is a very slight variation in the touchdown velocity (V_0) obtained by simulation and experiments, the experiments reporting a value of V_0 = 5 m/s whereas the simulation reports a value of V_0 = 5.05 m/s. The difference is because in the experiment, the wedge slides along a post and the friction between the sliding mechanism holding the wedge and the post reduces the velocity by a very small amount. After reaching the maximum penetration depth (entry phase), the buoyancy makes the wedge rebound (exit phase) till its vertical velocity becomes zero. Then it penetrates again due to its weight and this entry-exit cycle go on till the wedge comes to rest. The small oscillations in the experimental velocity curve were attributed to the vibration of the cord, as reported by Yettou *et al*. (2006).

The full motion simulations of the 25° wedge were performed for three touchdown velocities, V_0 = 6.26 m/s, 5.05 m/s and 4.43 m/s. The variations of the penetration depth (for the bottom most point or the apex of the wedge) and velocity with time are shown in Fig. 11. The maximum penetration depth corresponding to the touchdown velocities V_0 = 6.26 m/s, 5.05 m/s and 4.43 m/s are 0.393 m at t = 0.346 s, 0.359 m at t = 0.356 s and 0.342 m at t = 0.356 s respectively.

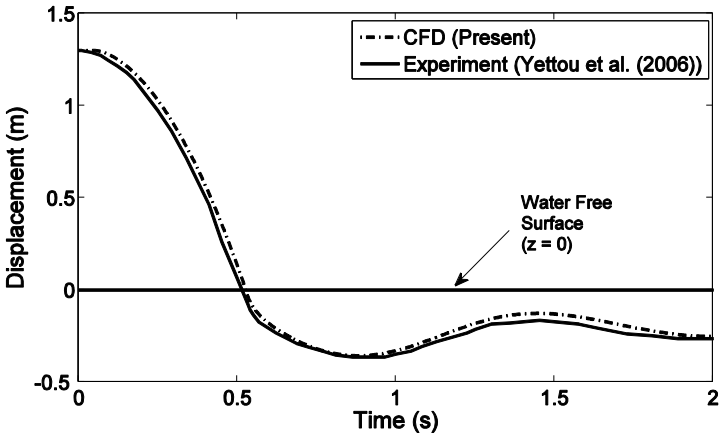

(a) Displacement variation with time (h = 1.3 m)

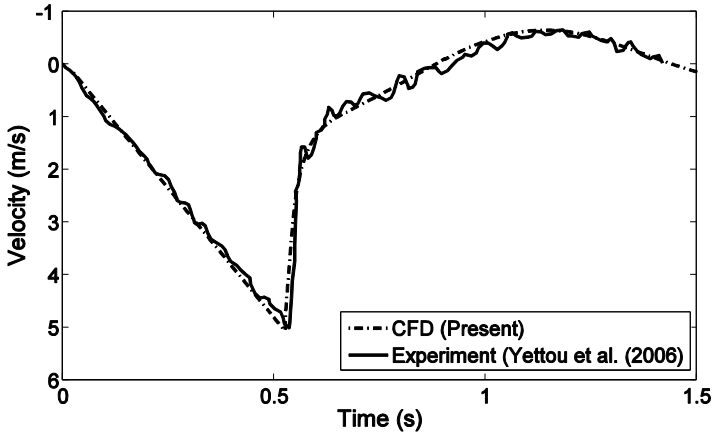

(b) Velocity variation with time (h = 1.3 m)

Fig. 10 Comparison of CFD results with experiments for full motion of 25° wedge

6. Discussion

The comparison of the results obtained from the present CFD simulation with experiments for water entry of wedges and cylinder are presented in Figs. 3, 4 and 10 brings out the following:

(i) The convergence study shows that to accurately predict the impact pressure and the slamming loads acting on the body shape a very fine mesh size (5 mm edge length) is required. In order to reduce the computational cost and to achieve practical size of the problem, an interaction region is defined closer to the body and in the region where the body interacts with fluid, where the finer mesh sizes are used and other regions are specified with coarser mesh sizes.

(ii) From Fig. 4, it is very clear that the peak pressure and the corresponding time instants predicted at different locations for initial stage water entry of a wedge are in excellent agreement with the experimental results. However, at P2 location, the quality of the peak pressure prediction is poor (about 16% less).

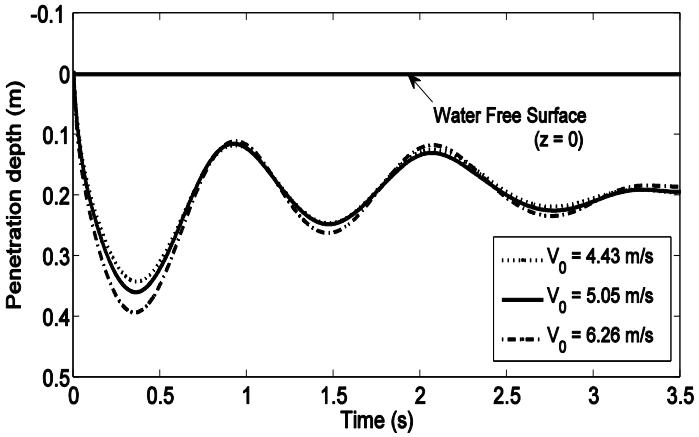

(a) Penetration depth variation with time

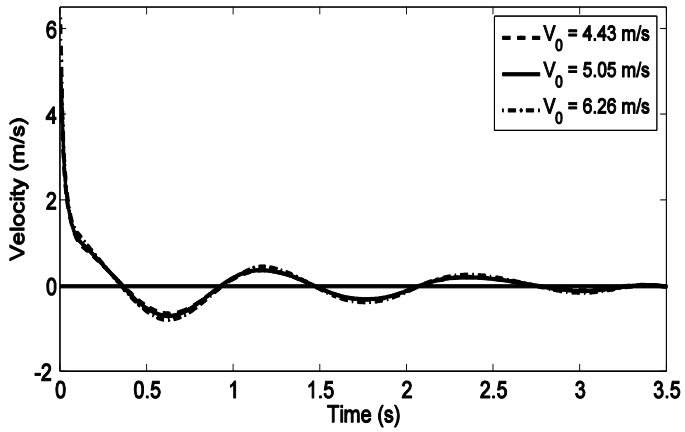

(b) Velocity variation with time

Fig. 11 CFD simulation results for the full motion of 25° wedge.

(iii) From Figs. 5-7, it can be concluded that as the touchdown velocity or the drop height increases, the impact force also increases but as the deadrise angle increases the impact force decreases. The effect of three-dimensional body on the water entry process is also bought out using the present study and it outlines the fact that near the ends of the wedge, the pressures are less than those near its midsection.

(iv) From Fig. 10 it is seen that the entire motion of the body in the entry, as well as rebound phases, has been simulated using the present CFD approach accurately. The displacement and velocity variation with time is in excellent agreement with the experimental results. The breaking of the free surface has also been predicted by the present CFD approach, though it could not be verified against experiments and is shown in Fig. 9.

(v) The nominal time step used in the present simulation is 2×10^{-5} s., with adaptive time stepping capability. A computational time of about 11 hours for 4.79 million cells (with fine mesh edge length of 5 mm) was recorded (in a PC with 3.2 GHz processor speed and 16 GB RAM) for the water entry of wedge for a total simulation time of 0.045 s.

The example problems treated here can also be modeled by 2D mesh and it has been verified that 2D calculations will yield the same results of all parameters except pressures, especially at the ends. This is because the symmetry of the wedges considered. The motivation of 3D calculations is to develop a methodology which can treat problems with (a) port-starboard asymmetry of wedge shape, (b) CG not being on the centre-plane and (c) the touchdown velocity has a nonzero horizontal component. The methodology presented in the present work can treat all such problems. In addition, the end effect that is predicted by 3D simulation (see Figs. 7 and 8) cannot be captured by 2D modeling.

7. Conclusions

CFD simulations have been carried to predict the impact pressure and the slamming loads on three-dimensional rigid wedges under the influence of gravity by solving Navier-Stokes equations utilizing the VOF scheme to keep track of the free surface. The simulation results have been validated with experimental results from the literature with excellent agreement. The influence of touchdown velocity on the water entry process was investigated in terms of the peak pressure and the slamming load (i.e., vertical force). Simulations were also carried out on water entry of wedges with various deadrise angles and its effect on both peak pressure and slamming loads have been estimated and validated with experiments. The three-dimensional features of pressure distribution on the body show that the end regions of the wedge suffer relatively lower impact pressures compared to the regions away from the ends. The results of CFD simulations of the entry as well as rebound (or exit) phases of a wedge have been compared with experimental results with reasonably good accuracy.

This paper, for the first time, reports the time variation of impact pressures on wedge using 3D CFD simulation and as a result is able to predict the longitudinal distribution of impact pressures on the wall of the wedge, which is a 3D effect. The experimental validations of all quantities, especially impact pressures in early times and trajectory in late times covering both entry and rebound phases, have been remarkably accurate. The results are sensitive to meshing strategy and time step and therefore effort has been made to arrive at general guidelines for meshing which is likely to yield accurate results.

References

Abrate, S. (2013), "Hull Slamming", *Appl. Mech. Rev*., **64**(6), 1-35.

Aquelet, N., Souli, M. and Olovsson, L. (2006), "Euler-Lagrange coupling with damping effects: application to slamming problems", *Comput. Method. Appl. M.*, **195**(1-3), 110-132.

Arhan, M., Deleuil, G. and Doris, C.G. (1978), "Experimental study of the impact of horizontal cylinders on a water surface", *Proceedings of the 10th Annual Offshore Technology Conference*, Houston, Texas, May.

Bisplinghoff, R.L. and Doherty, C.S. (1952), "Some studies of the impact of vee wedges on a water surface", *J. Franklin Inst*., ***253***, 547-560.

Campbell, I.M.C. and Weynberg, P.A. (1980), *Measurement of parameters affecting slamming*, Report No. 440, Wolfson Unit for Marine Technology, Technology Reports Center No.OTR-8042.

Carcaterra, A. and Ciappi, E. (2004), "Hydrodynamic shock of elastic structures impacting on the water: theory and experiments", *J. Sound Vib*., **271**, 411-439.

Chen, Q., Ni, B., Chen, S. and Tang, J. (2014),"Numerical simulation of the water entry of a structure in free fall motion", *J. Mar. Sci. Appl*., **13**, 173-177.

Chuang, S.L. (1966), *Slamming of rigid wedge shaped bodies with various deadrise angles*, DTMB Report No. 2268.

Colicchio, G., Greco, M., Miozzi, M. and Lugni, C. (2009), "Experimental and numerical investigation of the water-entry and water-exit of a circular cylinder", *Proceedings of the International Workshop on Water Waves and Floating Bodies*, Zelegonorsk, Russia.

Davis, M.R. and Whelan, J.R. (2007), "Computation of wet deck bow slam loads for Catamaran arched cross sections", *Ocean Eng*., **34**, 2265-2276.

Engle, A. and Lewis, R. (2003), "A comparison of hydrodynamic impacts prediction methods with two dimensional drop test data", *Mar. Struct*., **16**, 175-182.

Fairlie-Clarke, A.C. and Tveitnes, T. (2008), "Momentum and gravity effects during the constant velocity water entry of wedge shaped sections", *Ocean Eng*., **35**, 706-716.

Faltinsen, O.M. (2005), Hydrodynamics of High-Speed Marine Vehicles, Cambridge University Press.

FLOW3D user manual (2013), Version 10.1, Flow Science Inc.

Gong, K., Liu, H. and Wang, B.L. (2009), "Water entry of a wedge based on SPH model with an improved boundary treatment", *J. Hydrodynam.*, **21**(6), 750-757.

Greenhow, M. (1987), "Wedge entry into initially calm water", *Appl. Ocean Res*., **9**, 214-223.

Greenhow, M. and Lin, W.M. (1983), *Non-linear free surface effects: Experiments and Theory*, Report No. 83-19, MIT, Dept. of Ocean Engineering.

Judge, C., Troesch, A. and Perlin, M. (2004), "Initial water impact of a wedge at vertical and oblique angles", *J. Eng. Math*., **48**, 279-303.

Kleefsman, K.M.T., Fekken, G., Veldman, A.E.P., Iwanowski, B. and Buchner, B. (2005), "A volume-of-fluid based simulation method for wave impact problems", *J. Comput. Phys*., **206**, 363-393.

Korobkin, A.A. and Pukhnachov, V.V. (1988), "Initial stage of water impact", *Annu. Rev. Fluid Mech*., **10**, 159-185.

Lange, N.A. and Rung, T. (2011), "Impact tests in pure and aerated water", *Proceedings of the 30th International Conference on Ocean, Offshore and Arctic Engineering*, Rotterdam, Netherlands.

Lewis, S.G., Hudson, D.A., Turnock, S.R. and Taunton, D.J. (2010), "Impact of a free-falling wedge with water: synchronized visualization, pressure and acceleration measurements", *Fluid Dyn. Res*., **42**(3), 035509.

Lin, P. (2007), "A fixed-grid model for simulation of a moving body in free surface flows", *Comput. Fluids*, **36**, 549-561.

Lin, M.C. and Shieh L.D. (1997), "Flow visualization and pressure characteristics of a cylinder for water impact", *Appl. Ocean Res*., **19**(2), 101-112.

Luo, H.B., Wang, S. and Guedes Soares, C. (2011), "Numerical prediction of slamming loads on rigid wedge subjected to water entry using an explicit finite element method", (Eds., Guedes Soares C. and Fricke W.), Advances in Marine Structures. Taylor & Francis, UK.

Miao, G. (1989), *Hydrodynamic Forces and Dynamic Responses of Circular Cylinders in Wave Zones*. Ph.D. Thesis, Department of Marine Hydrodynamics, NTH, Trondheim.

Miloh, T. (1991), "On the initial-stage slamming of a rigid sphere in a vertical water entry", *Appl. Ocean Res*., **1**(1), 34-48.

Muzaferija, S., Peric, M., Sames, P.C. and Schellin, T.E. (1998), "A two fluid Navier-Stokes solver to simulate water entry", *Proceedings of the 22nd Symp. on Naval Hydrodynamics*, Washington D.C.

Nair, V.V. and Bhattacharyya, S.K. (2015), Water entry and exit of axisymmetric bodies by CFD approach. (under review).

Oger, G., Doring, M., Alessandrini, B. and Ferrant, P. (2006), "Two-dimensional SPH simulations of wedge water entries", *J. Comput. Phys*., **213**(2), 803-822.

Sarpkaya, T. (1978), "Wave impact loads on cylinders", *Proceedings of the 10th Annual Offshore Technology Conference*, Paper No. OTC 3065, Houston, Texas, May.

Sicilian, J.M. (1990), *A FAVOR based moving obstacle treatment for FLOW3D*, Flow Science Technical Note #23 (FSI-90-TN23), Flow Science Inc.

Stenius, I., Rosen, A. and Kuttenleuler, J. (2006), "Explicit FE-modeling of fluid-structure interaction in hull-water impacts", *Int. Shipbuild. Progress*, **53**(2), 103-121.

Tveitnes, T., Fairlie-Clarke, A.C. and Varyani, K. (2008), "An experimental investigation into the constant velocity water entry of wedge-shaped sections", *Ocean Eng*., **35**(14-15), 1463-1478.

Van Nuffel, D., Vepa, K.S., De Baere, I., Lava, P., Kersemans, M., Degrieck, J., De Rouck, J. and Van Paepegem, W. (2014), "A comparison between the experimental and theoretical impact pressures acting on a horizontal quasi-rigid cylinder during vertical water entry", *Ocean Eng*., **77**, 42-54.

von Karman, T. (1929), The impact of seaplane during landing, NACA TN 321.

Wagner, H. (1932), Phenomena associated with impacts and sliding on liquid surfaces, Zeitschrift für Angewandte Mathematik und Mechanik.

Wei, G. (2005), *A fixed mesh method for general moving objects*, Flow Science Technical Note #73 (FSI-05-TN73), Flow Science Inc.

Wu, G.X., Sun, H. and He, Y.S. (2004), "Numerical simulation and experimental study of water entry of a wedge in free fall motion", *J. Fluid. Struct.*, **19**, 277-289.

Yang, J.M. and Stern, F. (2009), "Sharp interface immersed-boundary/level- set method for wave-body interactions", *J. Comput. Phys*., **228**(17), 6590-6616.

Yang, Q. and Qiu, W. (2012a), "Numerical simulation of water impact for 2D and 3D bodies", *Ocean Eng.*, **43**, 82-89.

Yang, Q. and Qiu, W. (2012b), "Numerical solution of 3D water entry problems with a constrained interpolation profile method", *J. Offshore Mech. Arct*., **134**(4), 041101.

Yettou, E.M., Desrochers, A. and Champoux, Y. (2006), "Experimental study on the water impact of a symmetrical wedge", *Fluid Dyn. Res*., **38**(1), 47-66.

Zhang, Y., Zou, Q., Greaves, D., Reeve, D., Hunt-Raby, A., Graham, D., James, P. and Lv, X. (2010), "A level set immersed boundary method for water entry and exit", *Commun. Comput. Phys*., **8**(2), 265-288.

Zhao, R. and Faltinsen, O.M. (1993), "Water entry of two-dimensional bodies", *J. Fluid Mech*., **246**, 593-612.

Zhao, R., Faltinsen, O. and Aarsnes, J. (1996), "Water entry of arbitrary two-dimensional sections with and without separation", *Proceedings of the 21st Symposium on Naval Hydrodynamics*, Trondheim, Norway.

Zhu, X., Faltinsen, O.M. and Hu, C. (2007), "Water entry and exit of a horizontal circular cylinder", *J. Offshore Mech. Arct*., **129**(4), 253-264.

QM